Journal of the European Ceramic Society 21 (2001) 2471–2478

www.elsevier.com/locate/jeurceramsoc

Structure description of the thermic phase transformation sillimanite–mullite

S. Rahman*, U. Feustel, S. Freimann

Institut für Mineralogie, Universität Hannover, Welfengarten 1, 30167 Hannover, Germany

Abstract

The thermic phase transformation of sillimanite to 3:2 mullite was structurally examined with the main focus on the initial stage of this transfomation. Single crystals of very pure sillimanite were annealed for different time periods (1600 °C; 45 min–96 h) and then analyzed employing X-ray and electron microscopic investigations. Electron diffraction patterns showed decreasing intensities of the ⟨101⟩ reflections depending on the duration of thermal treatment. Dynamic effects causing the decrease of the 101 reflection could be excluded, because calculations of the dynamic electron diffraction intensities showed an intensity increase of the 101 reflection with increasing crystal thickness. Using the videographic reconstruction method the initial stage of the transformation (2–6 h, 1600 °C) of sillimanite to 3:2 mullite is characterized as follows: (1) Splitting of the oxygen sites, resulting in tetrahedra- and octahedra-tilts and/or rotations; (2) statistical distribution of Si and Al on the tetrahedral sites. The results of the videographic reconstruction were confirmed via videographic simulations. A prolonged period of thermal treatment (24 h, 1600 °C) leads to the complete transformation of sillimanite to 3:2 mullite with precipitations of amorphous SiO_2. This precipitation of partial melt appears in HRTEM images as white rectangles (approximately 20×20 nm) with edges parallel to ⟨110⟩.

Keywords: Disorder; Mullite; Point defects; Sillimanite; TEM

1. Introduction

The system Al_2O_3–SiO_2 is very important for silica ceramics which can be widely used in industries because of their good thermal, electrical and mechanical properties. The only intermediate phase in this system, arising in the subsolidus area and from the melt, is mullite $Al_2[Al_{2+2x}Si_{2-2x}]O_{10-x}$. Other Al_2SiO_5 modifications are andalusite, disthene and sillimanite.

The structures of mullite and sillimanite are similar in some aspects. Both structures consist of AlO_6 octahedra chains, which are linked with Si/Al tetrahedra double chains parallel to the *c*-axis (Fig. 1). In sillimanite, there is an ordered distribution of Si and Al on the tetrahedral sites, whereas in mullite this distribution is disordered and furthermore there exists another tetrahedral site (Al*), coupled with the occurrence of oxygen vacancies. The *c*-lattice constant of mullite has only half the size as in sillimanite. With the influence of high temperatures (>1200 °C) sillimanite transforms to mullite according to the phase diagram given by Holdaway.[1] Many authors examined this thermal transformation in order to understand its exact mechanism and kinetics. Holdaway[1] calculated the energy needed for the exchange of the Si and Al positions in sillimanite and stated that the degree of Si/Al disorder on the tetrahedral sites increases with increasing temperatures. This was confirmed by Greenwood,[2] who calculated the Gibbs free energy as a function of the Si/Al disorder at different temperatures. Gyepesova and Durovic[3] studied the thermal transformation of sillimanite at high temperatures (<1650 °C) and found the formation of several intermediate phases, though their diffraction patterns only showed the sillimanite reflections. Guse et al.[4] also described a metastable intermediate phase. They observed on single crystal pattern decreasing intensities of reflections with $l=2n+1$ in the progress of the transformation. This decrease of intensity was stated by Berger,[5] too, who took X-ray diffraction patterns of sillimanite single crystals heated under pressure. He interpreted this intensity decrease as progressive Si/Al disorder without a change in the chemical composition. In situ structure determinations of Winter and Ghose[6] yielded a decrease of the Al–O and Si–O distances. A TEM study of sillimanite

* Corresponding author.
E-mail address: s.rahman@mineralogie.uni-hannover.de (S. Rahman).

0955-2219/01/$ - see front matter
PII: S0955-2219(01)00386-7

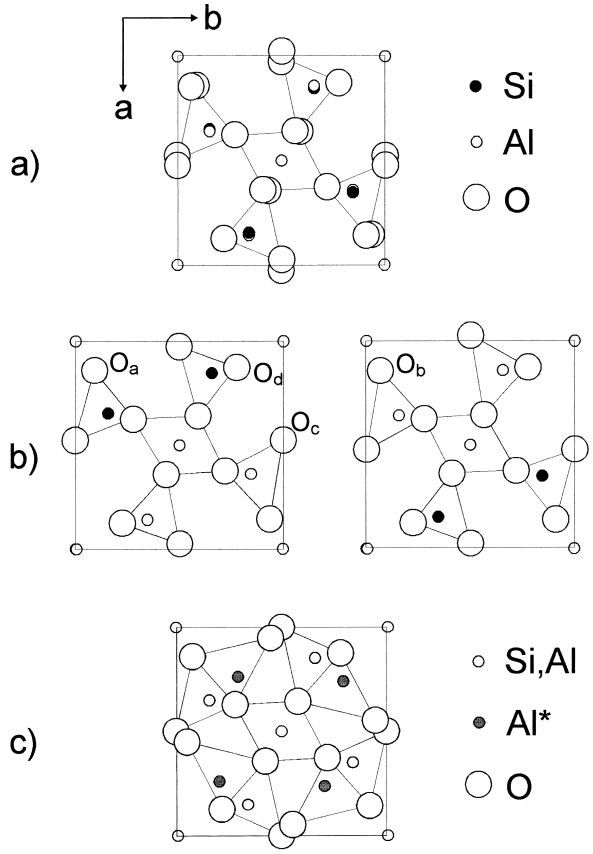

Fig. 1. (a) Structure of sillimanite.[6] (b) Structure of sillimanite subdivided in two parts, left $0 \leqslant z \leqslant 0.5$, right $0.5 \leqslant z \leqslant 1$. (c) Average structure of mullite.[15]

annealed for long time periods (1600 °C) shows oriented SiO_2-rich precipitations on the *ab*-plane.[7,8]

The investigations of the sillimanite–mullite transformation can only roughly explain the mechanism of the transformation until the present time. There are many contradictory assumptions concerning the thermic transformation. The exact structural processes could not be adequately described. The aim of the present study is to characterize the structure of "disordered sillimanite" at the initial stage of the thermal transformation of sillimanite to 3:2 mullite using electron diffraction and the videographic reconstruction procedure. Furthermore, the process of transformation was characterized by TEM investigations using samples annealed for different durations.

2. Experimental

The examined sillimanite was a clear single crystal of high purity in gem quality from Sri Lanka. Polarization microscope, electron microprobe and X-ray investigations did not show any impurities or inhomogenities. Several analyses by electron microprobe (Cameca Camebax MB) gave a chemical composition of 61.8 wt.% Al_2O_3 and 38.2 wt.% SiO_2, typical for sillimanite. Furthermore the trace elements Na, K, Fe, Mg and Ca could be detected. The lattice constants were $a = 7.488$ Å, $b = 7.681$ Å, $c = 5.776$ Å.

For the thermal treatment a high temperature stove (Nabertherm Supertherm HT 04/17) was used which can reach temperatures up to 1800 °C and has a Pt 30% Rh/Pt 6% Rh-thermoelement. The experiments were performed at 1600 °C varying the duration of thermal treatment (45 min–96 h). At the end of the annealing period the probes were immediately taken out of the stove and quenched at room temperature. Electron diffraction patterns and high resolution images were obtained with a Hitachi H-800 microscope, operating at 200 kV accelerating voltage. The microscope is equipped with a LaB_6 cathode and a top-entry high resolution specimen stage with a $\pm 10°$ tilting angle. Preparation of the crystallites for HREM investigations was carried out by crushing them with propanol in an agate mortar and transferring the suspension onto copper grids covered with a perforated carbon film.

Electron microprobe examinations showed increasing melt precipitation of the annealed sillimanite crystals with increasing annealing duration. Because of the small size of the precipitations (approximately 20×20 nm) an adequate analysis was not possible. After 24 h thermal treatment the chemical composition of the crystal has changed to 71.9 wt.% Al_2O_3 and 28.1 wt.% SiO_2, close to the composition of 3:2 mullite.

3. TEM investigations

In order to describe the initial stage of the sillimanite–mullite transformation HRTEM images and electron diffraction patterns were taken from sillimanite crystals with different annealing durations. Electron diffraction patterns of the *h*0*l* plane (Fig. 2) show remarkable changes in the intensities of the ⟨101⟩ reflections. The ⟨101⟩ reflection of the original sillimanite (without thermal treatment, Fig. 2a) has a relatively high intensity. In the diffraction pattern of the crystal annealed for 6 h (Fig. 2b) a strong decrease of the ⟨101⟩ reflection can be noticed. With increasing duration of thermal treatment the ⟨101⟩ reflections disappear and diffuse maxima around the ⟨101⟩ positions arise, which are typical for mullite. In Fig. 2d, corresponding to the completely to 3:2 mullite transformed sillimanite, these diffuse maxima at the positions $h = 2n \pm 2/3$, 0, $l = n + 1/2$ can be clearly recognized together with rounded diffuse streaks running approximately parallel to the c^*-axis. Since it is often possible to observe several transformation stages within one crystal, it can be assumed, that the transformation starts at several places in the crystal and continues with different speed.

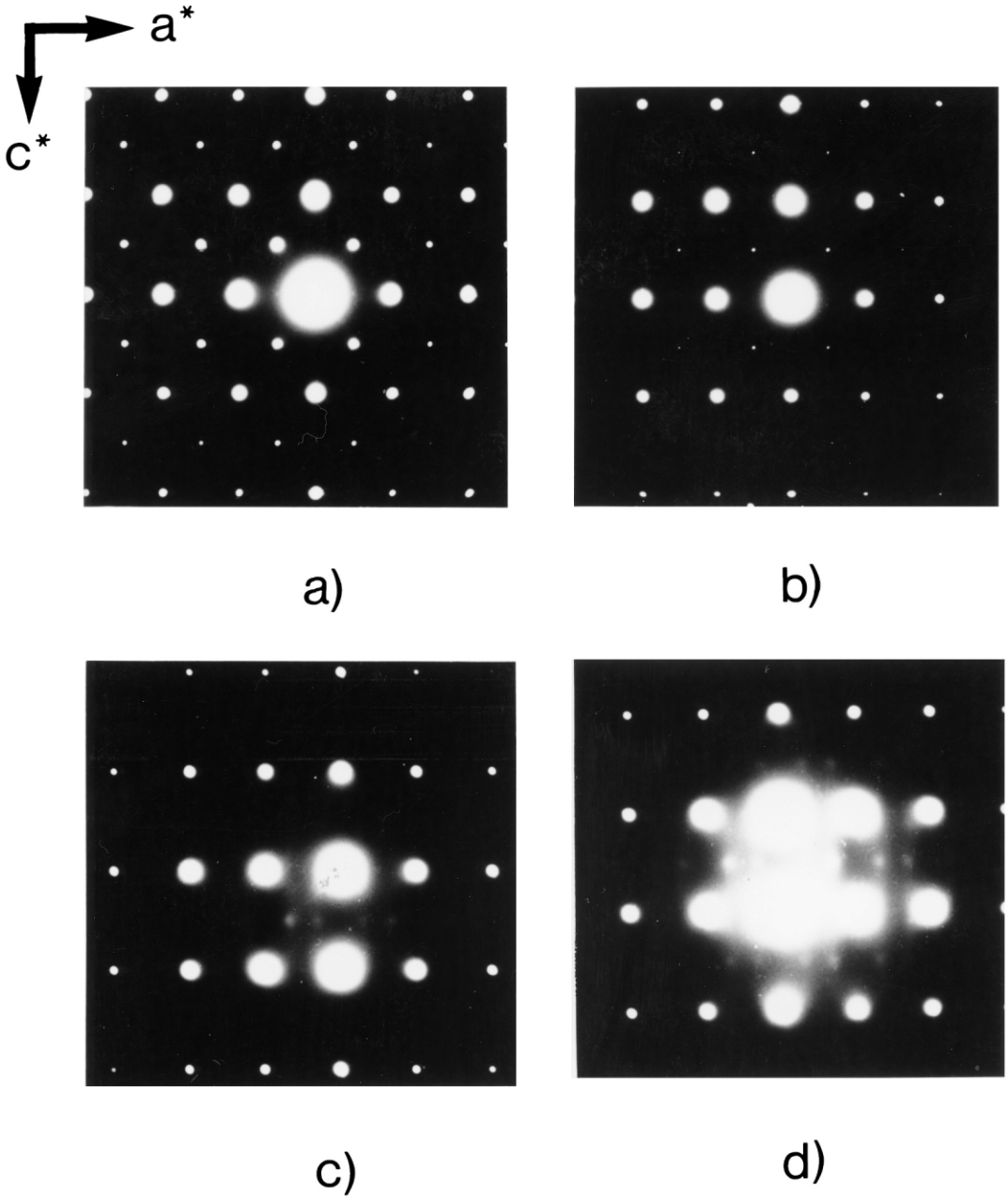

Fig. 2. Electron diffraction patterns of quenched sillimanite with different annealing times: (a) 0 h; (b) 6 h; (c) 12 h; (d) 96 h.

Whereas the electron diffraction patterns show remarkable changes in the intensities of the ⟨101⟩ reflection depending on the duration of thermal treatment, in HRTEM images no changes in the contrast can be observed.[7]

In the case of electron diffraction there are strong interactions between electron beam and crystal and therefore between the primary and the diffracted beams, too. This interaction depends on the thickness of the crystal. In order to prove that the intensity decrease of the ⟨101⟩ reflections is not caused by dynamic effects, the intensities of electron diffraction were calculated for different values of the crystal thickness using the multi-slice method.[9] In Fig. 3 the amplitudes of electron diffraction for the reflections 000, 002, 200 and 101 are presented in dependence on the crystal thickness. The dynamic calculations yielded that the intensity of the 101 reflection is increasing with increasing crystal thickness and therefore the observations in the experiment are not caused by dynamic effects. Consequently the intensity decrease of the ⟨101⟩ reflection is caused by certain changes of the atomic site parameters.

The thermal transformation of sillimanite to mullite proceeds via an intermediate stage, which is reached after a short duration of thermal treatment (about 2–6 h, 1600 °C). A longer period of thermal treatment (8–12 h)

shows the beginning of the formation of square-shaped regions as presented in Fig. 4. These regions still have a structure related to sillimanite. In the high resolution image no contrast variations can be seen, which indicate oxygen vacancies as shown by Rahman and Weichert[10] and Paulmann et al.[11] A prolonged thermal treatment leads to the complete transformation of sillimanite into 3:2 mullite with the precipitation of SiO_2. In HRTEM images of crystals annealed for at least 12 h (Fig. 5) with the beam directions [001] the white rectangles seem to be without any lattice fringes, probably due to the melt process. The edges of the rectangles are parallel to [110] or [−110] and can extend to 30 unit cells. Bright field images at low magnification for the *ab*- and *ac*-plane are given in Figs. 6 and 7, respectively. In Fig. 6 the rectangles are randomly distributed. In the *ac*-plane the rectangles are visible as ellipsoides elongated along the *c*-direction. Electron diffraction patterns of the *ac*-plane from such crystals as in Fig. 7 show a complete transformation to 3:2 mullite (Fig. 2d).

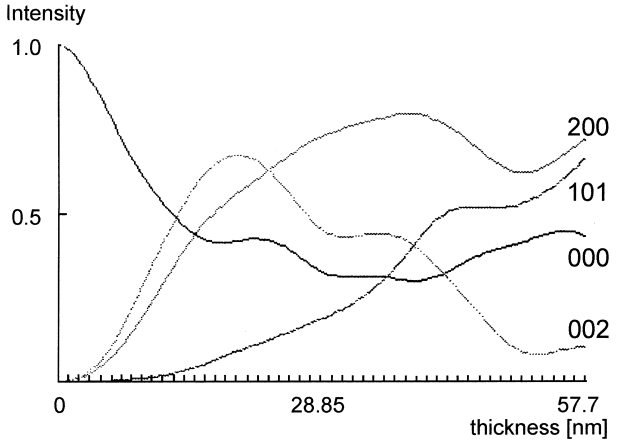

Fig. 3. Dependence of dynamical electron diffraction intensities on crystal thickness.

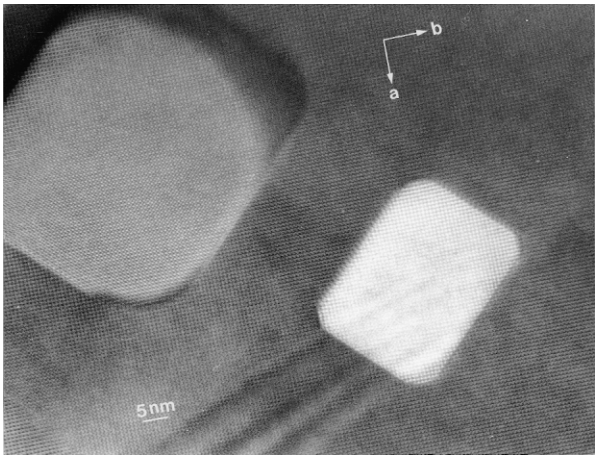

Fig. 4. HRTEM image of the *ab*-plane of sillimanite annealed for 8 h (200 kV, $c_s = 1$ mm, $c_c = 1.1$ mm, divergence $(\alpha) = 5{\cdot}10^4$ [rad]).

4. Videographic reconstruction

In order to determine the structural changes causing the decrease of the ⟨101⟩ reflection, the videographic reconstruction procedure was applied. The videographic reconstruction is—together with the videographic simulation—a very useful method for the determination of

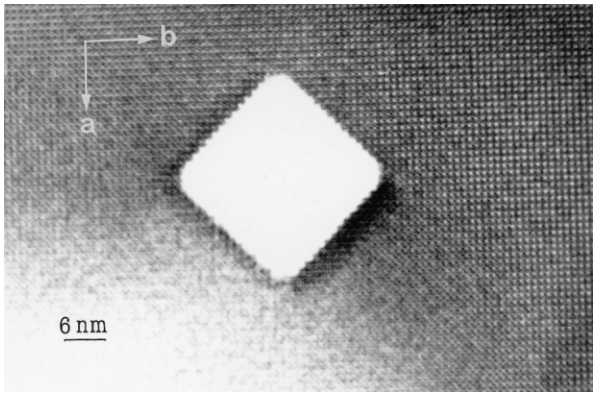

Fig. 5. HRTEM image of the *ab*-plane of sillimanite annealed for 12 h (200 kV, $c_s = 1$ mm, $c_c = 1.1$ mm, divergence $(\alpha) = 5{\cdot}10^4$ [rad]).

Fig. 6. Bright field image of the *ab*-plane of sillimanite annealed for 18 h.

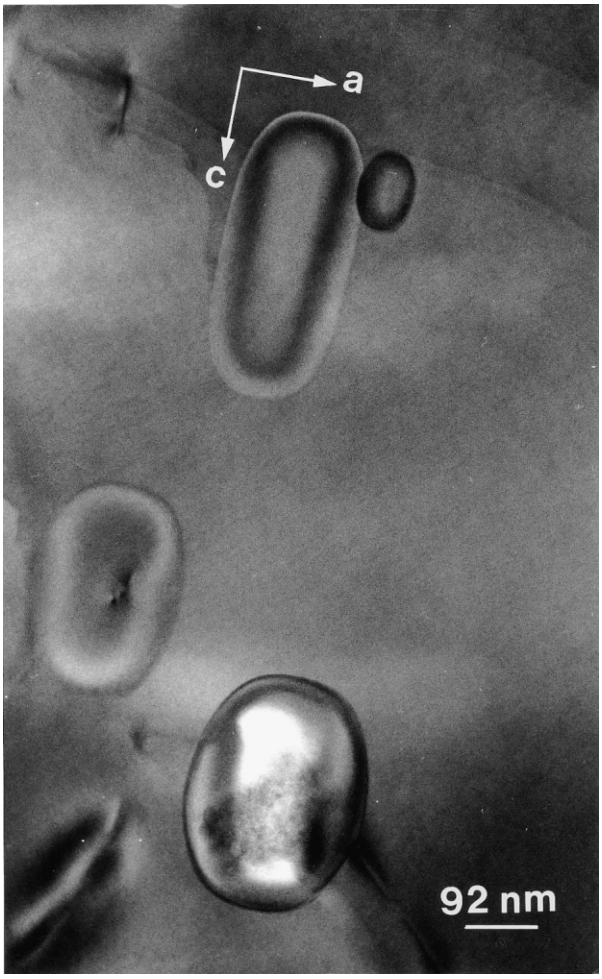

Fig. 7. Bright field image of the *ac*-plane of sillimanite annealed for 18 h.

the real structure in the case of disorder.[12,13] Whereas, with the videographic simulation, different structure models can be tested, the videographic reconstruction enables the recovery of real structure configurations by filter operations in reciprocal space. The principal idea in the reconstruction is that the diffuse regions of a partly ordered structure are a subset of the monotonous diffuse background for a random disorder. For this reason usually a randomly disordered structure is assumed as a starting model. Its Fourier transform shows, besides the Bragg peaks $Q(u, v)_B$ a diffuse background $\Delta Q(u, v)_d$. Image reconstruction of the real structure $\varphi(x, y)$ can be achieved by selective filtering of certain frequencies by means of the transfer function. In this case $Q(u, v)_B$ or $\Delta Q(u, v)_d$ can be multiplied by the transfer functions $G_1(u, v)$ and $G_2(u, v)$, respectively.[12]

$$\mathcal{F}[\varphi(x, y)] = Q(u, v)_B \cdot G_1(u, v) + \Delta Q(u, v)_d \cdot G_2(u, v). \quad (1)$$

The values of the transfer functions can be chosen to select either the diffuse regions, parts of the diffuse regions or the Bragg reflections which are accounted for by a backward Fourier transform. The transfer function can be expressed as a convolution (∗) between the reciprocal lattice function $F(u, v)$ and a window function $W(u, v)$, which determines the co-ordinates of the selected areas and corresponds to a filter mask.

$$G(u, v) = F(u, v) * W(u, v). \quad (2)$$

In the electron diffraction pattern of the *h*0*l* plane of "disordered sillimanite" mainly the intensity decrease of ⟨101⟩ was observed without a noticable contribution of diffuse scattering. In this special case the distribution of only one structure variant (the unit cell, Fig. 8a), generating a supercell, can be used as starting model. The Fourier transform of this supercell corresponds to the experimental diffraction pattern of the original sillimanite (without thermal treatment). In order to determine the variation in the sillimanite structure, which causes the decrease of the ⟨101⟩ reflections, the amplitude of the ⟨101⟩ reflections is reduced in the Fourier transform with the aid of the filter mask [Eq. (1)]. In the next step a backward Fourier transform of this reciprocal image is performed. The obtained reconstructed image of the real structure can be interpreted concerning the atomic positions and the occupation probabilities (corresponding to the grey level). Since in this special case the reconstruction is only applied to the amplitude of a Bragg reflection, the reconstructed image of the *ac*-plane consists of identical unit cells (Fig. 8b), which represent the average structure of the "disordered sillimanite" and show striking differences compared with the original elementary cell of sillimanite:

- the structure obtained by the videographic reconstruction exhibits additional atomic positions compared with the sillimanite structure, i.e. a splitting of the oxygen positions can be noted;
- instead of the ordered Si/Al distribution found in sillimanite, a randomly distribution can be observed.

The loss of the Si/Al order is marked in Fig. 8b by a medium grey level of the coinciding Si/Al position between the values for Si and Al. Therefore the oxygen positions O_c and O_d, co-ordinating the Si cation, are occupied as well as the O_c and O_d positions co-ordinating the Al cation in the sillimanite structure (Fig. 1). The O_a and O_b positions have very similar co-ordinates and cannot be distinguished in the videographic representation of the structure projected on the *ac*-plane.

The results of the videographic reconstruction have to be tested by videographic simulations. Since the ordered sequence of Si and Al in the tetrahedral double chains is no longer ensured, the ideal Si–O and Al–O atomic distances cannot be maintained. In the videographic simulation Al–O–Al and Si–O–Si linkages must be allowed in order to generate a disordered Si/Al distribution as

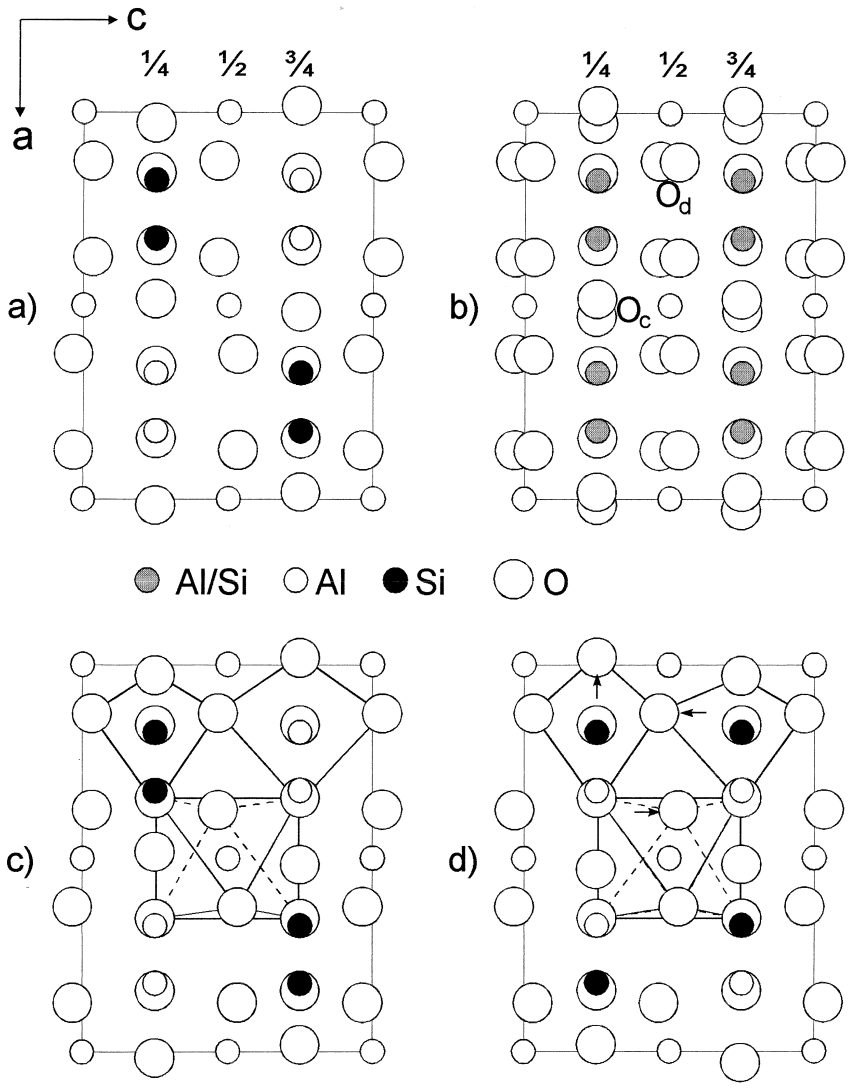

Fig. 8. (a) Sillimanite structure projected on (010). (b) Reconstructed average structure of "disordered sillimanite". (c) Regular SiO_4 and AlO_4 tetrahedra and AlO_6 octahedra in the ordered sillimanite structure. (d) Examples of distorted SiO_4 tetrahedra and AlO_6 octahedra in the structure of "disordered sillimanite".

indicated by the reconstruction. Whereas in the ordered sequence with Si–O–Al or Al–O–Si linkages, respectively, the occupation of the common oxygen site (O_c or O_d) is determined by the ideal bond length (Fig. 1), in the case of Si–O–Si or Al–O–Al linkages there is no preference in the occupation of both O_c or O_d split sites (Fig. 8). In this case an intermediate O site could be assumed. However, no such intermediate location of O_c or O_d was observed in the reconstructed structure image. Because there are no restrictions resulting from a coupled occupation of the Si/Al and the O_c and O_d positions, a great number of structure variants for the *ac*-plane can be derived from the average structure. In order to reduce this number, the unit cell is divided into 8 parts (Fig. 9), so that every structure variant contains only one cation and the co-ordinating oxygen atoms. The parts of the unit cell with the co-ordinates $0 \leqslant x \leqslant 1/4, z$ and $1/2 \leqslant x \leqslant 3/4, z$ can be represented with the variants 1–16 and the other parts (with the co-ordinates $1/4 \leqslant x \leqslant 1/2, z$ and $3/4 \leqslant x \leqslant 1, z$) with the variants 17–32. The variants contain either a Si or an Al cation and differ in the occupation of the oxygen sites.

With the aid of these structure variants a videographic simulation can be performed in order to check the results of the reconstruction. The variants are distributed via combination tables containing the combination probabilities.[12] In the combination tables the division of the unit cell is considered and the observance of the stoichiometry and crystal chemical rules (interatomic distances, co-ordination number). By an ordered distribution of only the variants 1, 9, 17 and 25 the sillimanite structure is achieved (Fig. 9). Preferring these combinations but allowing additionally combinations with the other variants (with low probabilities) a partly disordered distribution is generated. The Fourier transform of this simulation field shows a decrease of the

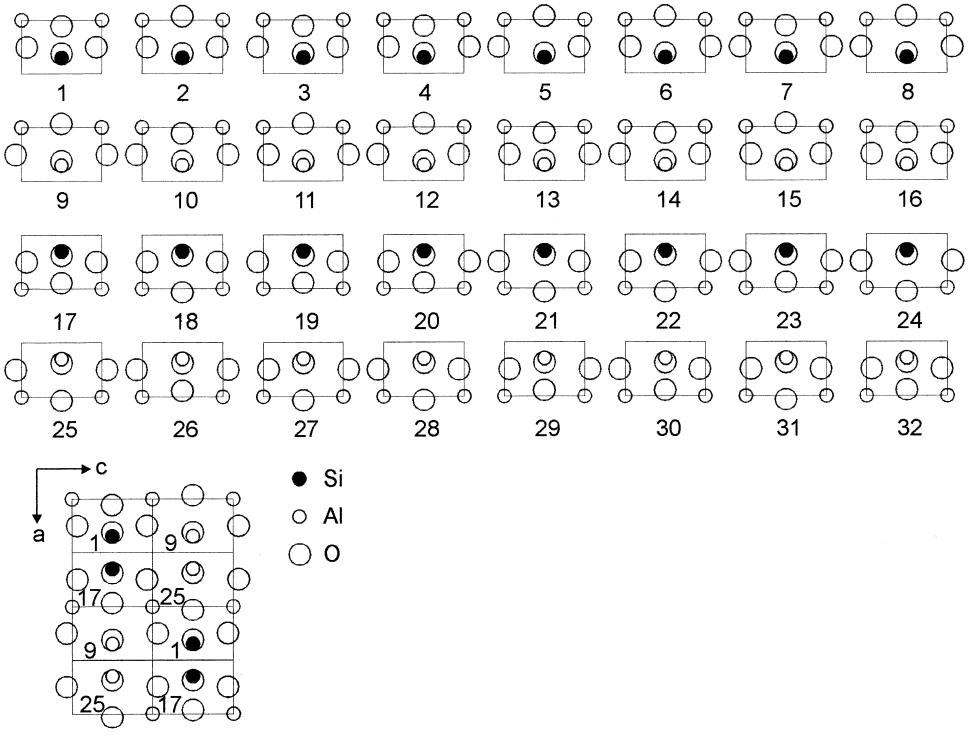

Fig. 9. Thirty-two structure variants for the *ac*-plane of "disordered sillimanite".

⟨101⟩ reflections and, therefore, the results of the videographic reconstuction are confirmed. A statistical distribution of all structure variants results in a Fourier transform, in which the ⟨101⟩ intensities are nearly zero.

By means of the presented results, the initial stage of the sillimanite–mullite transformation at 1600 °C can be characterized by a statistical distribution of Si and Al on the tetrahedral sites and distortions of the tetrahedra and octahedra (Fig. 8), resulting from the additional O_c and O_d sites.

5. Discussion

In the present investigation the videographic reconstruction method is used to determine the change in the sillimanite structure at the initial stage of the thermal transformation sillimanite–mullite by applying the filter operation to the ⟨101⟩ Bragg reflections. The most remarkable intensity variation was observed at the ⟨101⟩ reflection group. However, there are small intensity variations of other Bragg reflections, too, which are not considered in the present calculation. The videographic reconstruction method was mainly used to determine real structures in cases in which diffuse scattering occurs. The present examination revealed that the method can be also applied to Bragg reflections in order to evaluate the structure variation due to amplitude and phase changes of a certain Bragg reflection group.

Considering the results of the TEM investigations and the videographic reconstruction the kinetics of the thermal phase transformation of sillimanite to 3:2 mullite at 1600 °C can be described as follows.

The initial stage at short periods of thermal treatment (2–6 h, 1600 °C) is characterized by Si/Al disorder. In this stage there is a high mobility of ions, probably accompanied by the occupation of some Al* positions (like in mullite) as indicated in IR investigations by Rüscher.[14] With increasing duration of thermal treatment the diffusion process of Si and Al is accelerated forming regions with a higher SiO_2 content, which appear in the HRTEM image (Fig. 4) as white rectangles with sillimanite like fringes (Si-rich "sillimanite"). At the same time Al cations leave these regions and diffuse into the matrix. This can be described as a bidirectional diffusion process. In the progress of the diffusion process the eutectic composition is reached in the SiO_2-rich regions and a partial melting occurs. HRTEM images of this state (Fig. 5) show the melt precipitations as white rectangles without lattice fringes. The surrounding matrix consists only of 3:2 mullite.

This process is accelerated by impurities. If there are many impurities such as alkalines in the crystal, the appearance of Si/Al disorder starts at lower temperatures and proceeds faster. Since a crystal never is completely homogenous and faultless, the Si/Al disorder proceeds at different places of the crystal with different speed. Therefore, it can be explained, why in one crystal

several states of transformation can be simultaneously observed.

References

1. Holdaway, M. J., Stability of andalusite and the aluminum silicate phase diagram. *Am. J. Sci.*, 1971, **97**, 97–129.
2. Greenwood, H. J., Al^{IV}–Si^{IV} disorder in sillimanite and its effect on phase relations of the aluminum silicate minerals. *Geol. Soc. Am. Inc. Memoir*, 1972, **132**, 553–571.
3. Gyepesova, D. and Durovic, S., Single crystal study of thermal decomposition of sillimanite. *Silicaty*, 1977, **2**, 147–150.
4. Guse, W., Saalfeld, H. and Tjandra, J., Thermal transformation of sillimanite single crystals. *N. Jb. Min. Mh.*, 1979, **4**, 175–181.
5. Berger, R. M., *Aluminum–Silicon Ordering in Sillimanite and Mullite*. PhD thesis, Harvard University, 1979.
6. Winter, J. K. and Ghose, S., Thermal expansion and high temperature crystal chemistry of the Al_2SiO_5-polymorphs. *Am. Mineral.*, 1979, **64**, 573–586.
7. Feustel, U., *Strukturelle Beschreibung der thermischen Umwandlung von Sillimanit in Mullit*. PhD thesis, Universität Hannover, 1996.
8. Raterron, P., Carpenter, M. and Doukhan, J. C., A TEM investigation of experimentally annealed sillimanite: new constraints for the SiO_2–Al_2O_3 join. *Mineral. Mag.*, 2000, **64**(2), 247–254.
9. Cowley, J. M. and Moodie, A. F., The scattering of electrons by atoms and crystals. I. A new theoretical approach. *Acta Crystallogr.*, 1957, **10**, 609–619.
10. Rahman, S. H. and Weichert, H.-T., Interpretation of HREM images of mullite. *Acta Crystallogr.*, 1990, **B46**, 139–149.
11. Paulmann, C., Rahman, S. H. and Strothenk, S., Interpretation of mullite HREM images along [010] and [100]. *Phys. Chem. Minerals*, 1994, **21**, 546–554.
12. Rahman, S. H., The videographic method: a new procedure for the simulation and reconstruction of real structures. *Acta Crystallogr.*, 1993, **A49**, 56–68.
13. Rahman, S. H., Videographic reconstructions and simulation of the real Cu_3Au structure at various temperatures. *Z. Kristallogr.*, 1994, **209**, 315–321.
14. Rüscher, C. H., Thermal transformation of sillimanite single crystals to 3:2 mullite plus melt: investigations by polarized IR-reflection micro spectroscopy. *J. Eur. Ceram. Soc.*, 2001, **21**(14), 2463–2469.
15. Angel, R. J. and Prewitt, C. T., Crystal structure of mullite: a re-examination of the average structure. *Am. Mineral.*, 1476–1482.